Available online at www.sciencedirect.com
ScienceDirect
Trans. Nonferrous Met. Soc. China 34(2024) 1300−1310
Transactions of Nonferrous Metals Society of China
www.tnmsc.cn

Effect of inorganic anions on precipitation of desilication products based on low-temperature Bayer process

Ji-long LIU[1,2,3], Xiao-lin PAN[1,2,3], Hong-fei WU[1,2,3], Xian-lin HOU[2], Hai-yan YU[1,2,3]

1. Key Laboratory for Ecological Metallurgy of Multimetallic Mineral (Ministry of Education), Northeastern University, Shenyang 110819, China;
2. School of Metallurgy, Northeastern University, Shenyang 110819, China;
3. Key Laboratory for Recycling of Nonferrous Metal Resources (Shenyang), Shenyang 110819, China

Received 17 December 2022; accepted 7 April 2023

Abstract: The effect of inorganic anion impurities in sodium aluminate solution on the composition, structure and micro-morphology of desilication products (DSPs) based on the low-temperature Bayer process was systematically investigated via XRD, FT-IR, SEM and PSD methods. The sodalites with chloride-type, carbonate-type and nosean-type precipitate in the presence of chloride, sulfate and carbonate in solution, and the aluminate ions in DSPs are partly replaced by the incorporation of anion impurities. The binding capability of sulfate to the DSPs cage is stronger than aluminate, chloride and carbonate. The particle size, agglomeration degree and thickness of the circular lamellar structure of DSPs are increased by rising the concentration of anion impurities. The anions enhance the dissolution of the zeolite framework and the formation of tetradentate rings in sodalite, which promotes the transformation of zeolite to sodalite.

Key words: Bayer process; sodium aluminosilicate hydrate; inorganic anion; desilication; crystal structure

1 Introduction

The Bayer process is the primary method to extract alumina from bauxite, and more than 90% of the worldwide alumina is produced by this method [1,2]. The bauxites contain various silicate minerals, such as quartz, kaolinite, silica, and illite [3], most of which can dissolve into sodium aluminate solution during the digestion process (giving kaolinite as an example in Eq. (1)). A variety of sodium aluminosilicate hydrates, referred to desilication products (DSPs), are formed by the reactions of the silicon ions with sodium aluminate solution, as given in Eq. (2) [4,5]. According to the thermodynamic stability of crystal structure, the amorphous phase first precipitates by the desilication reactions and then converts into zeolite (ZEO), sodalite (SOD) and cancrinite (CAN) [6,7].

$$Al_2Si_2O_5(OH)_4+6OH^- = 2SiO_3^{2-}+2Al(OH)_4^-+H_2O \quad (1)$$

$$6SiO_3^{2-}+6Al(OH)_4^-+8Na^+ = Na_8(Al_6Si_6O_{24})\cdot yH_2O+12OH^-+(6-y)H_2O \quad (2)$$

The industrial sodium aluminate solution contains numerous anion impurities such as Cl^-, CO_3^{2-}, SO_4^{2-} and various organic ions, which mainly originate from bauxite, industrial water and additives [8,9]. The anion impurities with a high concentration increase the density and viscosity of solution and reduce the quality of decomposed aluminum hydroxide [10]. Furthermore, the anion impurities can be incorporated into the aluminosilicate cage to form DSPs with different anion proportions ($Na_8(Al_6Si_6O_{24})\cdot X\cdot yH_2O$, in which X is $2Cl^-$, $2OH^-$,

Corresponding author: Xiao-lin PAN, E-mail: panxl@smm.neu.edu.cn
DOI: 10.1016/S1003-6326(24)66472-1

CO_3^{2-}, SO_4^{2-} [11]. According to the study of WHITTINGTON et al [12], the ability of anions to enter into the DSPs cage follows the order of OH^-, $Al(OH)_4^-$, Cl^-, CO_3^{2-} and SO_4^{2-}. PENG et al [13] studied the effects of anion impurities on the DSPs precipitation in aluminate solution with a high caustic ratio (4 mol/L NaOH, 0.5 mol/L $NaAl(OH)_4$), and reported that CO_3^{2-} and SO_4^{2-} promote the transformation from the amorphous phase to SOD. The stable CAN is precipitated at a higher reaction temperature (above 240 °C) and longer reaction time, and the conversion process from SOD to CAN is enhanced in the presence of CO_3^{2-} and SO_4^{2-} [14]. However, Cl^- has little effect on the DSPs transformation in the temperature range of 200−220 °C [15].

Previous studies generally reported the formation and transition of DSPs in industrial sodium aluminate solution with multiple anions using bauxite and silica-bearing minerals [16,17]. Nevertheless, the effect mechanisms of the single anion on the precipitation of DSPs were rarely reported. Furthermore, most studies were focused on the precipitation of DSPs in sodium aluminate solution with a high caustic ratio, but those with a low caustic ratio were still not well-defined. Therefore, the effects of various anion impurities on the composition, crystal structure and morphology of DSPs precipitated in sodium aluminate solution with a low caustic ratio were systemically investigated using soluble silicate as the silicon source by simulating the low-temperature Bayer process.

2 Experimental

2.1 Solution preparation

The sodium aluminate solution was prepared using the analytic reagents of NaOH, $NaAlO_2$ and $Na_2SiO_3·9H_2O$ from the Sinopharm Chemical Reagent Co., Ltd., and the analytic reagents of NaCl, Na_2SO_4 and Na_2CO_3 were used as the sources of inorganic anions. The mixed slurry was heated at 90 °C for approximately 2 h. The final solution was filtered through a caustic-resistant membrane in a pressure filter. The initial concentration of the solution was as follows: the caustic alkali (in the form of Na_2O) was 143.6 g/L, the alumina concentration was 108.2 g/L, and the silica concentration was 5.0 g/L. The concentrations of alumina and caustic alkali in synthetic solution were determined by the EDTA complexometric titration and acid-base titration, respectively. The concentration of SiO_2 was analyzed by the silicon−molybdenum blue spectrophotometry [18].

2.2 Synthesis of desilication products

The NaCl, Na_2CO_3 and Na_2SO_4 reagents were directly added into sodium aluminate solution to synthesize the slurries with various anion concentrations (in forms of Cl^-, CO_3^{2-} and SO_4^{2-}). The DSPs were synthesized at 145 °C in a silicone-oil-heated autoclave with bombs. The temperature control accuracy was ±1 °C, and the bombs were rotated at 50 r/min. The slurry was filtered after the desilication, and the solid was washed with hot water until the attached ions were utterly cleaned and then dried at 90 °C for 12 h. The desilication efficiency (η_{SiO_2}) of sodium aluminate solution was calculated by Eq. (3):

$$\eta_{SiO_2}=\frac{C_0-C_1}{C_0}\times 100\% \tag{3}$$

where C_0 and C_1 denote the concentration of SiO_2 in the sodium aluminate solution before and after the desilication process, respectively.

2.3 Characterization of solids

The particle size distribution of DSPs was determined by a laser particle size analyzer (PSD, Malvern Hydro 3000). The ultrasonic level was 90% of intensity for 10 min, and the stirrer speed was 990 r/min. The precipitated solids were analyzed by a powder X-ray diffractometer (XRD, Philips X'Pert PW3040−60) with Cu K_α radiation at 40 kV and 40 mA. The 2θ range was from 5° to 90°, and the scanning rate was 5 (°)/min. The proportions of various crystalline phases in DSPs were calculated by quantitative analysis [19]. The vibrational spectra of DSPs were obtained by an infrared spectrometer (FT-IR, IRAffinity-1). The solids were dispersed on conductive adhesive, sputtered with Au, and observed by a scanning electron microscope (FESEM, Zeiss Ultra Plus).

3 Results

3.1 Effect of inorganic anions on desilication degree

The silica concentrations after desilication

with various anion impurities and desilication efficiencies of sodium aluminate solution are illustrated in Fig. 1. As the anion concentration increases, the silica concentration significantly reduces and the corresponding desilication efficiency increases, indicating that the desilication reactions are improved by the inorganic impurities. However, the effect of anion impurities on the desilication efficiency is diminished when the concentration increases, which is consistent with the results of GOMES et al [20]. In the presence of SO_4^{2-}, the desilication efficiency of sodium aluminate solution reaches above 95%, and the SiO_2 concentration in the solution is lower than 0.35 g/L. Based on the thermodynamics and dynamics, the silica concentration results from a complex balance between the dissolution of silicon ions and re-precipitation of DSPs [21]. The results demonstrate that increasing the concentration of anion impurities can promote the precipitation of DSPs and improve the desilication degree.

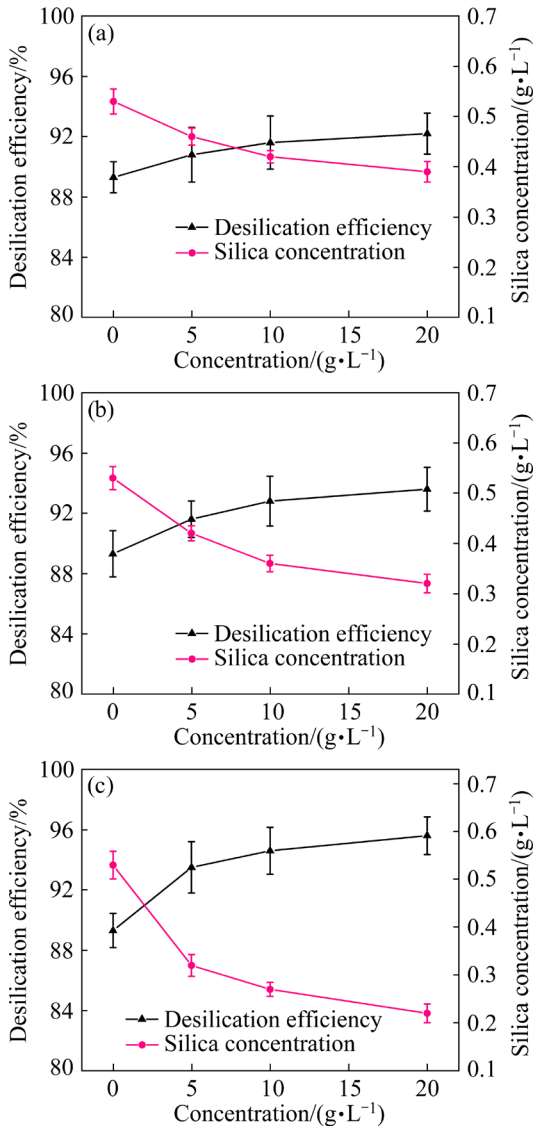

Fig. 1 Desilication efficiency of sodium aluminate solution with different anion impurity concentrations: (a) Chloride; (b) Carbonate; (c) Sulfate

The chemical compositions of DSPs precipitated with different anion concentrations are given in Table 1, and the formulas of DSPs were also calculated by the method proposed by WHITTINGTON et al [12], where C, S and Cl were assumed to exist as CO_3^{2-}, SO_4^{2-} and Cl^- within the precipitates. With the increase of anion concentration, the contents of SiO_2 and anions in DSPs are increased, demonstrating that the capability of DSPs to capture the anion impurities is strengthened. The incorporation of anion impurities via substitution reduces the adsorption capacity of DSPs for aluminate ions. The inorganic anion impurities are beneficial to the increase of the silica saturation coefficient of DSPs, which reduces the consumption of Al_2O_3 and Na_2O during the Bayer desilication process. Moreover, the molar mass of CO_3^{2-} in DSPs is more than that of Cl^- and SO_4^{2-} due to its large size and high charge density [22]. Thus, the bonding ability of the anion impurities with the silicate framework in DSPs is as follows: SO_4^{2-}, Cl^-, and CO_3^{2-}.

3.2 Effect of anion impurities on crystal structure of DSPs

The XRD patterns of DSPs precipitated with various anion concentrations are illustrated in Fig. 2. As shown in Fig. 2(a), the crystalline phases in the DSPs without anion impurity are ZEO and SOD, which are similar to the industrial DSPs [15]. The content and crystallinity of SOD are lower than those of ZEO due to the inefficient conversion from ZEO to SOD. The A-type zeolite phase was not observed in any XRD patterns, which is different from the DSPs precipitated at atmospheric pressure [23]. In addition, a characteristic broad hump in 2θ region of 17°−20° indicates that the crystallinity of DSPs is poor. The ZEO, SOD and chloride-type sodalite (SOD-Cl, $Na_8[Al_6Si_6O_{24}]Cl_2\cdot 6H_2O$) are the main phases in the presence of Cl^- anion, as presented in Fig. 2(b). The distinct peak of SOD-Cl is present in the 2θ range of 35°−40°, and its intensity is enhanced as the Cl^- concentration increases. The SOD is wholly transformed into the carbonate-type sodalite (SOD-C,

Table 1 Chemical composition of DSPs precipitated with various anion impurity concentrations

Anion impurity	Concentration/ ($g \cdot L^{-1}$)	Chemical composition/%				Calculated DSPs formula
		Al_2O_3	SiO_2	Na_2O	Anion	
Cl^-	0	34.91	31.33	18.52	–	$0.87Na_2O \cdot Al_2O_3 \cdot 1.53SiO_2 \cdot 2.64H_2O$
	5	33.39	31.58	19.51	2.65	$1.01Na_2O \cdot Al_2O_3 \cdot 1.71SiO_2 \cdot 0.24NaCl \cdot 1.94H_2O$
	10	32.28	32.32	19.79	2.98	$1.06Na_2O \cdot Al_2O_3 \cdot 1.81SiO_2 \cdot 0.28NaCl \cdot 1.93H_2O$
	20	31.75	33.31	19.88	3.29	$1.09Na_2O \cdot Al_2O_3 \cdot 1.89SiO_2 \cdot 0.32NaCl \cdot 1.92H_2O$
CO_3^{2-}	5	31.66	32.57	21.38	2.10	$1.17Na_2O \cdot Al_2O_3 \cdot 1.85SiO_2 \cdot 0.11Na_2CO_3 \cdot 1.96H_2O$
	10	31.25	33.08	21.41	2.27	$1.19Na_2O \cdot Al_2O_3 \cdot 1.90SiO_2 \cdot 0.13Na_2CO_3 \cdot 1.95H_2O$
	20	31.01	35.61	21.55	2.66	$1.21Na_2O \cdot Al_2O_3 \cdot 2.07SiO_2 \cdot 0.15Na_2CO_3 \cdot 1.92H_2O$
SO_4^{2-}	5	32.71	32.95	20.72	5.45	$1.11Na_2O \cdot Al_2O_3 \cdot 1.81SiO_2 \cdot 0.18Na_2SO_4 \cdot 1.69H_2O$
	10	31.51	34.63	20.86	6.02	$1.15Na_2O \cdot Al_2O_3 \cdot 1.97SiO_2 \cdot 0.21Na_2SO_4 \cdot 1.67H_2O$
	20	30.34	38.24	21.08	6.46	$1.21Na_2O \cdot Al_2O_3 \cdot 2.27SiO_2 \cdot 0.23Na_2SO_4 \cdot 1.66H_2O$

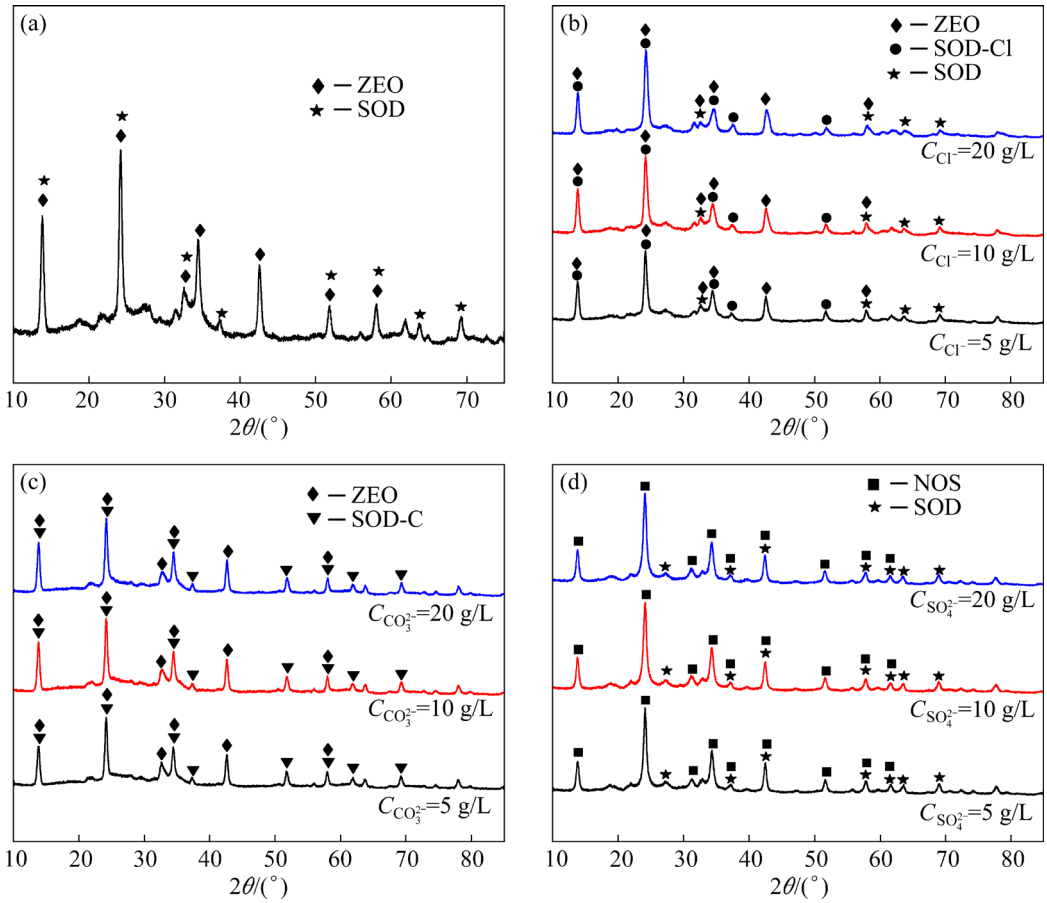

Fig. 2 XRD patterns of DSPs precipitated with various anion impurity concentrations: (a) No impurity; (b) Chloride; (c) Carbonate; (d) Sulfate

$Na_6[Al_6Si_6O_{24}] \cdot Na_2CO_3 \cdot 6H_2O$) when the CO_3^{2-} anion is present, as shown in Fig. 2(c). Moreover, the peak intensities of SOD-C in the 2θ ranges of 35°−40° and 60°−65° are enhanced by the increase of CO_3^{2-} concentration, while the peak intensities of ZEO are weakened. According to Fig. 2(d), the ZEO in the DSPs is eliminated when the SO_4^{2-} anion is present, and the silicate-bearing phases are converted into SOD and nosean-type sodalite (NOS, $Na_6[Al_6Si_6O_{24}] \cdot Na_2SO_4 \cdot 6H_2O$). The SOD and NOS have the similar silicate frameworks, and their thermodynamic stability is better than that of ZEO.

The above results illustrate that the SO_4^{2-} anion is beneficial to the transformation from the aluminosilicate phase to the stable DSPs [24].

Based on the XRD data shown in Fig. 2, the lattice parameters of DSPs were calculated by the Rietveld refinement method. The crystal structure of SOD without anion impurity is cubic, and its lattice parameter (a=b=c) is 0.8994 nm. The lattice parameters of SOD-Cl and SOD-C are 0.8995 nm and 0.8996 nm when the concentrations of Cl^- and CO_3^{2-} are all 10 g/L, demonstrating that Cl^- and CO_3^{2-} have little effect on the lattice parameters of SOD. However, the lattice parameter of NOS is 0.9017 nm, indicating that the lattice parameters of DSPs are primarily affected by the content and radius of doped ions, and the sequence follows the order of Cl^-, CO_3^{2-} and SO_4^{2-}.

Table 2 presents the proportions of different crystalline phases in DSPs calculated by the Rietveld method from the XRD data [19]. As the initial anion concentration increases, the content of ZEO shows a decreasing trend, and the proportion of SOD with anion substitution increases significantly. This indicates that the anion impurities can promote the transition from ZEO to SOD. Moreover, the SO_4^{2-} anion is conducive to the formation of NOS with low solubility during the desilication process. The NOS becomes more dominant than SOD as SO_4^{2-} anion concentration increases.

The infrared spectra of DSPs precipitated with different anion concentrations are shown in Fig. 3. The absorption band centered at 432 cm^{-1} is assigned to stretching vibration of Si—O (Al—O)

Table 2 Proportions of crystalline DSPs precipitated with various anion impurity concentrations (%)

Anion	Concentration/ ($g·L^{-1}$)	ZEO	SOD	SOD-Cl	SOD-C	NOS
Cl^-	5	63.6	15.6	20.8	−	−
	10	62.5	8.2	29.3	−	−
	20	60.0	5.3	34.7	−	−
CO_3^{2-}	5	80.1	−	−	19.9	−
	10	75.2	−	−	24.8	−
	20	72.2	−	−	27.8	−
SO_4^{2-}	5	−	21.6	−	−	78.4
	10	−	16.4	−	−	83.6
	20	−	10.4	−	−	89.6

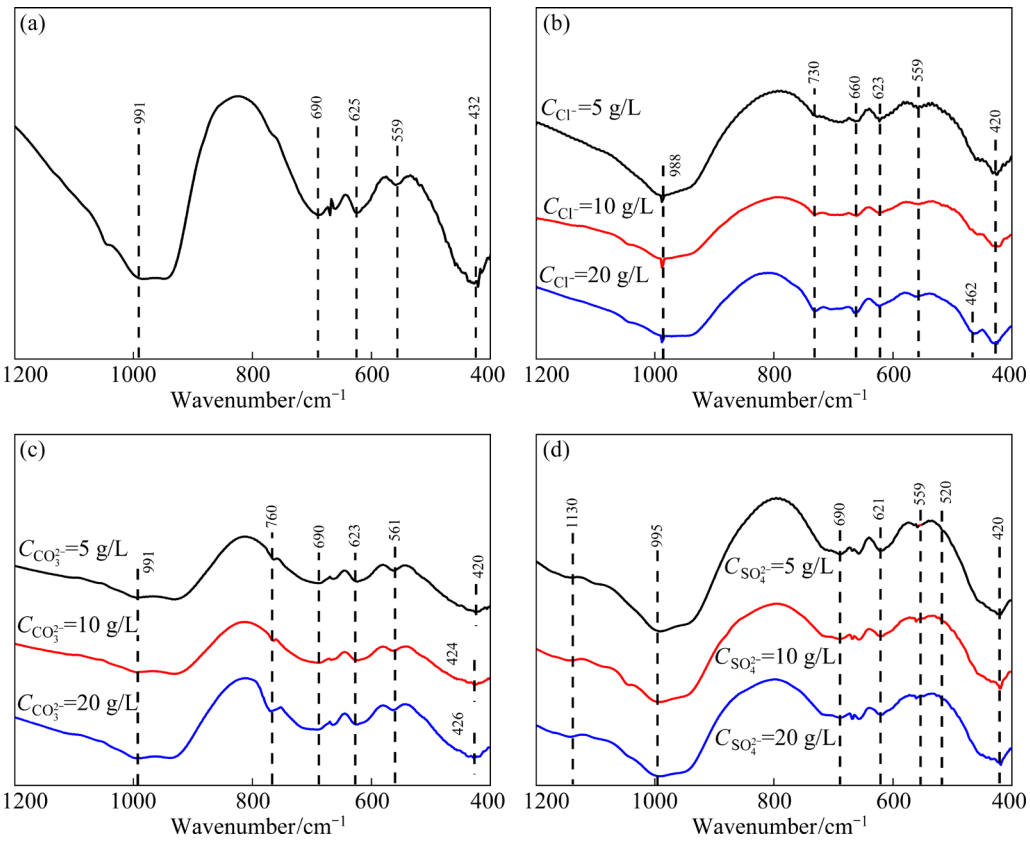

Fig. 3 Infrared spectra of DSPs precipitated with different anion impurity concentrations: (a) No impurity; (b) Chloride; (c) Carbonate; (d) Sulfate

bonds. The weak absorption band at 559 cm^{-1} is allocated to the double quadrangle ring vibration of the tetrahedron of silicon and aluminum, while the strong absorption band centered at 625 cm^{-1} is assigned to the symmetrical stretching absorption band of Al—O—Al bonds in Al/Si tetrahedron. The absorption band centered at approximately 691 cm^{-1} corresponds to the symmetric stretching of Si—O—Si bonds. For the 950−1000 cm^{-1} regions, the absorption bands are analogous to those obtained in natural SOD, which corresponds to the stretching and bending vibration of multicomponent aluminosilicate rings [25].

In Fig. 3(b), the absorption band at 420 cm^{-1} is assigned to the bending vibration of the Si—O (Al—O) bonds. The absorption band at 420 cm^{-1} shifts to the high-frequency regions with the increase of anion concentration, indicating that the high anion impurities promote the formation of Si—O bonds [26]. The absorption band centered at 462 cm^{-1} corresponds to the bending vibration of Al—O and Si—O bonds. Moreover, the samples exhibit some weak bands at 660 and 730 cm^{-1} due to the stretching vibration of Cl^-, and the corresponding intensity is enhanced as the Cl^- concentration increases. The sharp absorption bands centered at 988 cm^{-1} belong to the tetrahedron stretching vibration of Cl—Na_4 [27]. The weak bands at 760 and 520 cm^{-1} are assigned to the asymmetric bending of CO_3^{2-} (Fig. 3(c)) and SO_4^{2-} (Fig. 3(d)), respectively [28]. As the SO_4^{2-} concentration increases, the bands at 1130 cm^{-1} are sharper, indicating that the existence of SO_4^{2-} contributes to the formation and transformation of NOS.

3.3 Effect of anion impurities on morphology of DSPs

The morphology of the DSPs precipitated with various anion impurities is shown in Fig. 4, and the corresponding EDS results are given in Table 3. The DSPs without anion impurity are mainly composed of individual spherical particles with a diameter of larger than 1 μm, as shown in Fig. 4(a). The wool-cluster structure is composed of many concentric lamellae with a thickness of approximately 100 nm, which is the characteristic morphology of zeolite [26]. In the industrial production process, the DSPs are generally present as a polycrystalline feature due to the precipitation and re-dissolution growth mechanism, and some DSPs directly precipitate on the surface of existing minerals. Similarly, some SOD particles in this study are also precipitated between the lamellar structure and attached to the surface of ZEO in the desilication process in the synthetic aluminate solution (Fig. 4(b)), representing a mixture of distinct crystal morphology. In Fig. 4(c), the Cl^- anion promotes the formation of DSPs with a spherical morphology. However, it was not observed in sodium aluminate solution with a high caustic ratio when kaolinite was used as the silica source [14]. Figure 4(d) shows that the SOD particles in DSPs are more than those without anion impurity, implying that Cl^- can promote the formation of SOD. The CO_3^{2-} anion enhances the agglomeration degree, and individual crystallites are observed on the surface of larger particles due to the secondary nucleation, as shown in Fig. 4(e). Similar to the previous studies [21], the formation of SOD promotes the formation of interconnected clusters. More visible agglomeration (Fig. 4(h)) reveals the dominance of the SOD phase in DSPs. Regardless of synthesis conditions, although the DSPs exhibit similar morphology, the thicknesses of lamellae are different.

The EDS results illustrate that the anion impurities effectively replace the aluminate or hydroxide ions in DSPs. The alumina loss can be mitigated by remaining the aluminate and hydroxide ions in the solution. Although the anion impurity incorporation is only around 5%, the anion impurities stabilize the SOD phase and remove the additional silicate from the solution. The substitution of anion impurities reduces the alkalinity of DSPs, which is conducive to the resourceful treatment of bauxite residue. However, the DSPs with anions combine more silicates, and then the equivalent soda is lost for charge balance.

The particle size distribution of DSPs with various anion impurity concentrations is shown in Fig. 5. The overall size distribution of DSPs without anion impurity is relatively uniform, as shown in Fig. 5(a), and the average particle size is 50 μm. In the presence of Cl^- anion, the average particle size of DSPs increases to 80 μm (Fig. 5(b)). A small amount of CO_3^{2-} anion in the DSPs cage has little effect on the extent of agglomeration, and the particle distribution is uniform (Fig. 5(c)). The particle size of DSPs continues to increase to 100 μm in the presence of SO_4^{2-} (Fig. 5(d)).

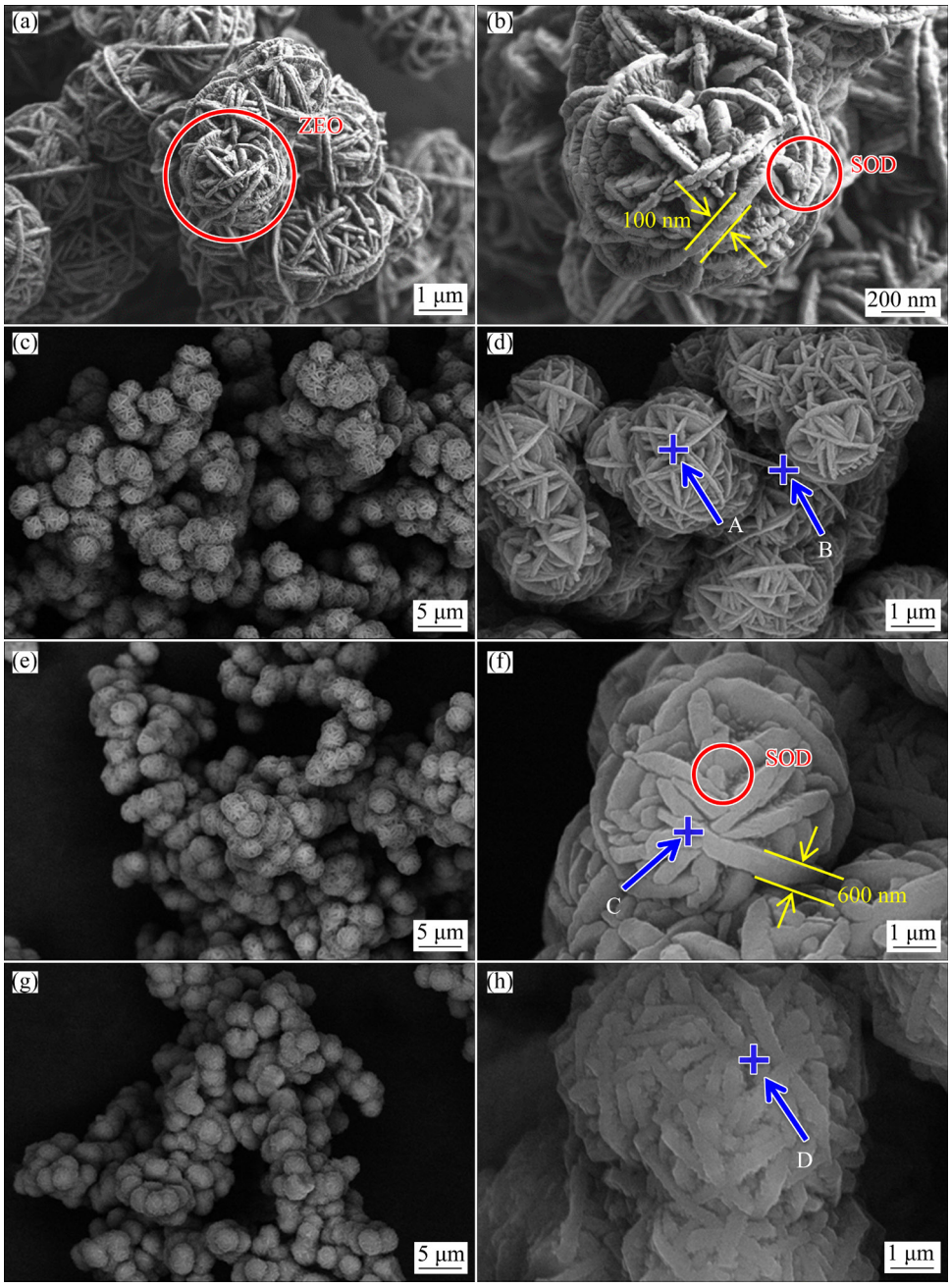

Fig. 4 SEM images of DSPs precipitated with 10 g/L anion impurity concentration: (a, b) No impurity; (c, d) Chloride; (e, f) Carbonate; (g, h) Sulfate

Table 3 EDS results corresponding to Fig. 4 (at.%)

Point	O	Na	Al	Si	Cl	C	S
A	57.13	12.14	13.31	14.97	2.45	–	–
B	57.04	12.07	13.25	13.38	4.26	–	–
C	56.83	11.02	12.44	14.19	–	5.52	–
D	57.69	11.64	10.53	14.03	–	–	6.11

According to the results from PENG and VAUGHAN [29], the particle size distribution of DSPs is related to crystal growth. When the anion impurity concentration is in the range of 0−20 g/L, the silica concentration displays an initial decline followed by a plateau. The silica concentration in the flat zone corresponds to the equilibrium concentration range of SOD, and the solute tends to be consumed by crystal growth rather than nucleation. As the anion concentration increases, the viscosity and diffusion layer thickness of sodium aluminate solution increase [22], which results in the DSP crystallines to aggregate into the larger particles.

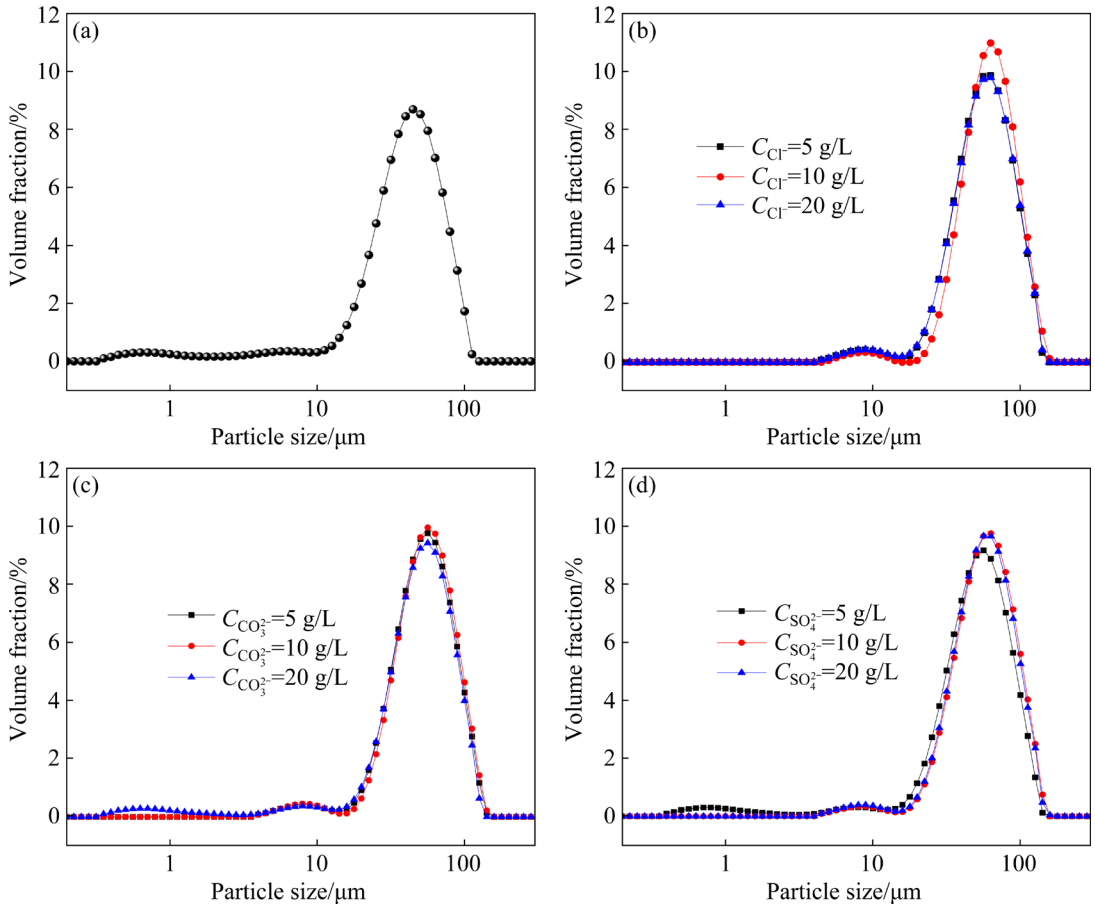

Fig. 5 Particle size distributions of DSPs precipitated with various anion impurity concentrations: (a) No impurity; (b) Chloride; (c) Carbonate; (d) Sulfate

4 Discussion

This study aimed to reveal the relationship between the inorganic anions and the precipitation characteristic of DSPs, which contributes to controlling the Bayer desilication process. The SO_4^{2-} content in DSPs is slightly higher than that of Cl^- and CO_3^{2-} when the initial anion impurity concentrations are the same. This illustrates that the SO_4^{2-} has a stronger bonding capability for the DSPs structure and is easily incorporated, which also predicts a low SO_4^{2-} concentration in the solution after desilication reactions.

The lattice parameters of DSPs are increased by the incorporation of anion impurities due to their larger ion radii. In the presence of SO_4^{2-}, the lattice parameters of DSPs increase significantly because of its higher incorporation. The incorporation of anion impurities into the DSPs cage dramatically decreases the content of ZEO. Although the anion impurities do not belong to the aluminosilicate cage structure of DSPs, their incorporation promotes the stability of the SOD structure. According to the Ostwald rule, the anion impurities enhance the transformation from an unstable state to a thermodynamically stable state [6,18]. The higher content of NOS in DSPs confirms that the ability of SO_4^{2-} to promote the phase transformation is more significant than that of Cl^- and CO_3^{2-}. The FT-IR results further elucidate the strong interaction between anion impurities and the DSPs cage. The characteristic bands show the substitution of anion impurities for aluminates, indicating that the binding ability of anion impurities to the DSPs cage is more potent than that of aluminate ions, which is consistent with the previous studies [13]. The characteristic woolly-ball structure [22] was observed when the soluble silicate was used. However, the morphology of DSPs was sheet-like and shows irregular aggregation when the kaolinite was used. The difference is most probably due to different reaction mechanisms. In the work of VOGRIN et al [14], the starting material is kaolinite,

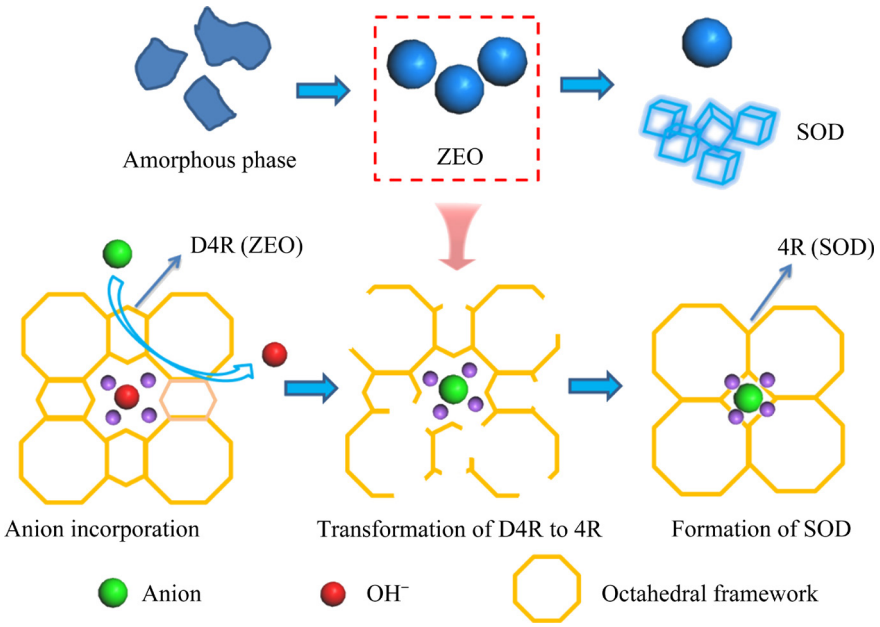

Fig. 6 Phase transformation mechanism from ZEO to SOD in presence of anion impurities

and the temperature range is 150−250 °C. The complex composition of kaolinite can significantly promote the secondary nucleation. Moreover, the growth mechanism of the dissolution and re-precipitation also causes an irregular aggregation morphology of DSPs.

Based on the above results, the phase transformation mechanism from ZEO to SOD in the presence of anion impurities is proposed, as summarized in Fig. 6. At the beginning, the aqueous silicate species precipitate as the amorphous phase. Under the synthetic conditions without anion impurity, these particles further aggregate into the larger amorphous particles and follow the classic nucleation−crystal growth route to convert to the ZEO phase with a double tetradentate ring (D4R) [30]. Subsequently, the ZEO is converted into SOD for a long time. The inorganic anion impurities promote the dissolution of the ZEO framework and the transformation of D4R to 4R, which accelerates the nucleation and growth of SOD.

5 Conclusions

(1) The aluminate ions in DSPs are partly replaced by the incorporation of anion impurities, which reduces the adsorption capacity of the DSPs cage for aluminate ions. The SO_4^{2-} has a stronger bonding capability for the structure of DSPs and is easier to incorporate into the DSPs than Cl^- and CO_3^{2-}.

(2) The particle size, thickness of the circular lamellar and the agglomeration degree of DSPs increase with the increase of anion impurity concentration. The lattice parameters of DSPs are increased by the incorporation of anion impurities.

(3) The anion impurities promote the dissolution of ZEO framework and the formation of tetradentate ring in SOD, which accelerates the nucleation and growth of SOD.

CRediT authorship contribution statement

Ji-long LIU: Investigation, Data curation, Writing − Original draft, Writing − Review and editing; **Xiao-lin PAN:** Validation, Supervision, Funding acquisition, Writing − Review; **Hong-fei WU:** Formal analysis, Data curation, Supervision; **Xian-lin HOU:** Conceptualization, Methodology; **Hai-yan YU:** Investigation, Visualization, Resources.

Declaration of competing interest

The authors declare that they have no known competing financial interests or personal relationships that could have appeared to influence the work reported in this paper.

Acknowledgments

The authors greatly appreciate the financial supports from the National Key R&D Program of China

(No. 2022YFC2904401), the National Natural Science Foundation of China (Nos. 22078055, 52074083, 51774079) and the Fundamental Research Funds for the Central Universities, China (No. N2225002).

References

[1] HIND A R, BHARGAVA S K, GROCOTT S C. The surface chemistry of Bayer process solids: A review [J]. Colloids and Surfaces A: Physicochemical and Engineering Aspects, 1999, 146(1/2/3): 359−374.

[2] GRAFE M, POWER G, KLAUBER C. Bauxite residue issues: III. Alkalinity and associated chemistry [J]. Hydrometallurgy, 2011, 108: 60−79.

[3] LI Xiao-bin, WANG Yi-lin, ZHOU Qiu-sheng, QI Tian-gui, LIU Gui-hua, PENG Zhi-hong, WANG Hong-yang. Reaction behaviors of iron and hematite in sodium aluminate solution at elevated temperature [J]. Hydrometallurgy, 2018, 175: 257−265.

[4] SMITH P. The processing of high silica bauxites−Review of existing and potential processes [J]. Hydrometallurgy, 2009, 98: 162−176.

[5] YANG Hui-bin, PAN Xiao-lin, YU Hai-yan, SUN jun-min. Dissolution kinetics and mechanism of gibbsitic bauxite and pure gibbsite in sodium hydroxide solution under atmospheric pressure [J]. Transactions of Nonferrous Metals Society of China, 2015, 25(12): 4151−4159.

[6] LIU Gui-hua, DONG Wen-bo, QI Tian-gui, ZHOU Qiu-sheng, PENG Zhi-hong, LI Xiao-bin. Behavior of calcium oxalate in sodium aluminate solutions [J]. Transactions of Nonferrous Metals Society of China, 2017, 27(8):1878−1887.

[7] REYES C A R, WILLIAMS C, ALARCÓN O M C. Nucleation and growth process of sodalite and cancrinite from kaolinite-rich clay under low-temperature hydrothermal conditions [J]. Journal of Materials Research, 2013, 16(2): 424−438.

[8] ZHENG K, GERSON A R, ADDAI-MENSAH J, SMART R S C. The influence of sodium carbonate on sodium aluminosilicate crystallisation and solubility in sodium aluminate solutions [J]. Journal of Crystal Growth, 1997, 171(1/2): 197−208.

[9] MACHOLD T, MACEDI E, LAIRD D W, MAY P M, HEFTER G T. Decomposition of bayer process organics: Low-molecular-weight carboxylates [J]. Hydrometallurgy, 2009, 99: 51−57.

[10] CHOI H S, KIM H W, LEE D H, YOON J, YUN C Y, CHAE K B. Scheduling algorithms for two-stage reentrant hybrid flow shops: minimizing makespan under the maximum allowable due dates [J]. International Journal of Advanced Manufacturing Technology, 2009, 42: 963−973.

[11] ZHANG Bai-yong, PAN Xiao-lin, WANG Jiang-zhou, YU Hai-yan, TU Gan-feng. Reaction kinetics and mechanism of calcium oxide in dilute sodium aluminate solution with oxalate based on lime causticization [J]. Transactions of Nonferrous Metals Society of China, 2019, 29(6): 1312−1322.

[12] WHITTINGTON B I, FLETCHER B L, TALBOT C. The effect of reaction conditions on the composition of desilication product (DSP) formed under simulated Bayer conditions [J]. Hydrometallurgy, 1998, 49: 1−22.

[13] PENG H, DING M L, VAUGHAN J. The anion effect on zeolite LTA to sodalite phase transformation [J]. Industrial and Engineering Chemistry Research, 2018, 57: 4−24.

[14] VOGRIN J, SANTINI T, PENG H, VAUGHAN J. The anion effect on sodium aluminosilicates formed under Bayer process digestion conditions [J]. Hydrometallurgy, 2020, 192: 1−9.

[15] ARMSTRONG J A, DANN S E. Investigation of zeolite scales formed in the Bayer process [J]. Microporous and Mesoporous Materials, 2000, 41(1): 89−97.

[16] SU Shuang-qing, MA Hong-wen, CHUAN Xin-yun. Hydrothermal synthesis of zeolite A from K-feldspar and its crystallization mechanism [J]. Advanced Powder Technology, 2016, 27: 139−144.

[17] RADOMIROVIC T, SMITH P, SOUTHAM D, TASHI S, JONES F. Crystallization of sodalite particles under Bayer-type conditions [J]. Hydrometallurgy, 2013, 137: 84−91.

[18] PAN, Xiao-lin, YU Hai-yan, TU Gan-feng, BI Shi-wen. Effects of precipitation activity of desilication products (DSPs) on stability of sodium aluminate solution [J]. Hydrometallurgy, 2016, 165: 261−269.

[19] PESCE C, PESCE G L, MOLINARI M, RICHARDSON A. Effects of organic additives on calcium hydroxide crystallisation during lime slaking [J]. Cement and Concrete Research, 2021, 139: 1−13.

[20] GOMES J F, DAVIES M, SMITH P, JONES F. The formation of desilication products in the presence of kaolinite and halloysite–The role of surface area [J]. Hydrometallurgy, 2021, 203: 1−12.

[21] BARNES M C, ADDAI-MENSAH J, GERSON A R. The kinetics of desilication of synthetic spent Bayer liquor and sodalite crystal growth [J]. Colloids and Surfaces A: Physicochemical and Engineering Aspects, 1999, 147: 283−295.

[22] WU Hong-fei, PAN Xiao-lin, YU Hai-yan, BI Shi-wen. Effect of carbonate on desilication of sodium aluminate solution at high temperature [J]. JOM, 2021, 73: 1180−1187.

[23] JIANG Tao, PAN Xiao-lin, WU Yan, YU Hai-yan, TU Gan-feng. Mineral transition of desilication products precipitated in synthetic sodium aluminate solution under atmospheric pressure [J]. Transactions of Nonferrous Metals Society of China, 2018, 28(2): 367−375.

[24] VOGRIN J, SANTINI T, PENG H, VAUGHAN J. Influence of chloride on sodium aluminosilicate solubility in Bayer liquor [J]. Microporous and Mesoporous Materials, 2020, 299: 1−8.

[25] XU B, SMITH P, WINGATE C, SILVA L D. The effect of calcium and temperature on the transformation of sodalite to cancrinite in Bayer digestion [J]. Hydrometallurgy, 2010, 105: 75−81.

[26] SU Shuang-qing, MA Hong-wen, CHUAN Xin-yun. Hydrothermal decomposition of K-feldspar in KOH−NaOH−H_2O medium [J]. Hydrometallurgy, 2015, 156: 47−52.

[27] HETTMANN K, WENZEL T, MARKS M, MARKL G. The sulfur speciation in S-bearing minerals: new constraints by a combination of electron microprobe analysis and DFT

calculations with special reference to sodalite-group minerals [J]. American Mineralogist, 2012, 97(10): 1653−1661.
[28] TANAKA H, EGUCHI H, FUJIMOTO S, HINO R. Two-step process for synthesis of a single phase Na-A zeolite from coal fly ash by dialysis [J]. Fuel, 2006, 85: 1329−1334.
[29] PENG H, VAUGHAN J. Aluminate effect on desilication product phase transformation [J]. Journal of Crystal Growth, 2018, 492: 84−91.
[30] ZHAN Yu-zhong, LI Xiao-xu, ZHANG Yong-guang, HAN Li, CHEN Yi-liang. Phase and morphology control of LTA/FAU zeolites by adding trace amounts of inorganic ions [J]. Ceramics International, 2013, 39: 5997−6003.

无机阴离子对低温拜耳法中脱硅产物析出的影响

刘吉龙[1,2,3]，潘晓林[1,2,3]，吴鸿飞[1,2,3]，侯宪林[2]，于海燕[1,2,3]

1. 东北大学 多金属共生矿生态化冶金教育部重点实验室，沈阳 110819；
2. 东北大学 冶金学院，沈阳 110819；
3. 沈阳市有色金属资源循环利用重点实验室，沈阳 110819

摘　要：利用 XRD、FT-IR、SEM 和 PSD 等手段系统研究无机阴离子对低温拜耳法过程中脱硅产物(DSPs)的组成、结构以及微观形貌的影响。当溶液中存在氯化物、硫酸盐和碳酸盐时，形成氯化物型方钠石、碳酸盐型方钠石和黝方石，部分铝酸盐离子被阴离子杂质取代。硫酸盐与 DSPs 的结合能力强于铝酸盐、氯化物和碳酸盐。随着阴离子浓度的增加，DSPs 的粒径增大，且 DSPs 的团聚程度和圆形片层结构的厚度均有所增加。此外，阴离子杂质会促进沸石骨架的溶解和方钠石中四元环的形成，从而促进沸石向方钠石转化。

关键词：拜耳法；水合铝硅酸钠；无机阴离子；脱硅；晶体结构

(Edited by Bing YANG)